

# Unifying KV Cache Compression for Large Language Models with LeanKV

Yanqi Zhang<sup>1\*</sup> Yuwei Hu<sup>1\*</sup> Runyuan Zhao<sup>1</sup> John C.S. Lui<sup>2</sup> Haibo Chen<sup>3</sup>

<sup>1</sup>Huawei <sup>2</sup>The Chinese University of Hong Kong <sup>3</sup>Shanghai Jiao Tong University

## Abstract

Large language models (LLMs) exhibit exceptional performance but incur significant serving costs due to their substantial memory requirements, with the key-value (KV) cache being a primary bottleneck. Existing KV cache compression techniques, such as quantization and pruning, apply uniform treatment to both keys and values, and discard unimportant tokens entirely, overlooking the fine-grained differences in significance of various components within the KV cache. To address these limitations, we introduce *LeanKV*, a framework that advances KV cache compression by exploiting three levels of differentiation in the KV cache: (1) the differing impact of keys and values on attention computation, (2) the varying importance of tokens, and (3) the diverse dynamic sparsity patterns across attention heads. At the core of LeanKV is an on-GPU memory manager that compacts fragmented free memory list into contiguous regions in parallel, effectively translating sparsity in the KV cache into performance gains. We evaluate LeanKV on several mainstream models, including the recent "thinking model". LeanKV is able to compress the KV cache by  $2.7\times$  to  $5.7\times$  with near-lossless accuracy on complex workloads requiring sophisticated reasoning and long-generation capabilities, and enhances throughput by  $1.9\times$  to  $5.4\times$ .

## 1 Introduction

Large language models (LLMs) like GPT [4, 9, 46] and Gemini [57] have demonstrated significant potential to impact our daily lives, offering promising applications in areas including chatbots [12, 59], programming [21, 24], mathematics [50, 71] and medical assistance [49, 65]. Despite their exceptional performance, hosting LLMs is costly due to their large model sizes, demanding extensive hardware resources. Given the pervasive adoption of LLMs, enhancing serving efficiency has become critically important [6, 18, 25, 31, 36, 47, 53, 68].

LLMs are fundamentally based on the Transformer architecture [61, 62], which employs the attention mechanism to generate tokens sequentially, based on the input prompt and previously generated tokens. Within the attention mechanism, each token is transformed into query, key and value feature vectors. The attention scores, derived from the dot product of the query and key vectors, enable the model to weigh the significance of different tokens. Subsequently, the output is computed as the weighted sum of the value vectors, based on the attention scores. To capture diverse relationships between

tokens, the attention mechanism is typically divided into multiple heads [5, 51, 61]. Each head independently computes attention, and their outputs are concatenated and transformed to create a richer representation of the input data.

To avoid redundant computation, LLM inference frameworks typically cache intermediate key and value tensors in memory, commonly referred to as the KV cache [32]. The size of the KV cache scales linearly with both sequence length and the number of concurrent requests, often comprising over 90% of total memory consumption [19, 32, 66, 67]. As state-of-the-art models continue to support longer sequences [4, 17, 30, 38, 57, 60], and with the rise of recent "thinking models" [23, 29, 58] that generate extended reasoning processes, the KV cache has emerged as a critical bottleneck for LLM serving efficiency. It limits the number of concurrent requests that can fit in memory and increases attention computation latency due to its memory bandwidth-bound nature [14, 15].

Recognizing the critical role of the KV cache in limiting serving efficiency, researchers have investigated various compression techniques, primarily focused on quantization [2, 27, 37] and pruning [10, 20, 35, 64, 69]. Quantization reduces the size of the KV cache by converting floating-point feature values into integers, representing them based on pre-defined intervals. Pruning, on the other hand, reduces the token sequence length by eliminating unimportant tokens based on attention scores. While promising, these techniques overlook the fine-grained differentiation in the significance of various KV cache components, limiting their overall effectiveness. First and foremost, existing quantization methods save key and value vectors of all tokens at a uniform precision, disregarding the distinct roles of keys and values and the varying importance of tokens. Second, current pruning methods employ static memory allocation across attention heads, neglecting the dynamic and heterogeneous attention patterns observed across heads and requests. Moreover, these pruning methods have not been comprehensively evaluated on workloads requiring advanced reasoning, such as programming and mathematics.

In this paper, we present *LeanKV*, a framework that advances KV cache compression by leveraging three levels of differentiation within the KV cache:

**1. Differentiated Keys and Values.** LeanKV assigns higher precision to key vectors than to value vectors, based on the observation that key vectors play a more significant role in attention computations.

**2. Token Importance Differentiation.** Guided by attention scores, LeanKV stores tokens at varying precision levels

\*Equal contribution.

based on their significance. Most critical tokens are quantized at higher precision, less critical tokens are quantized at lower precision, and the least significant tokens are pruned. This hierarchical approach enables a flexible tradeoff between model accuracy and memory efficiency.

**3. Per-head Dynamic Sparsity.** Attention score distributions exhibit dynamic sparsity across both heads and requests. Within a single request, the number of critical tokens varies across heads, and for the same head, the number of critical tokens also varies across different requests. To address this variability, LeanKV dynamically identifies critical tokens per-head, per-request, adapting memory allocation accordingly.

These differentiations within the KV cache pose new challenges in memory management. In LeanKV, each request requires varying amounts of memory for each attention head to store tokens at different precision levels. Moreover, key and value vectors of the same token are compressed at different precisions. These complexities significantly increase memory management overhead, compared to traditional attention mechanisms, where memory allocation is uniform across all heads.

To address these challenges, LeanKV employs an on-GPU memory manager that efficiently handles the irregular memory usage patterns across heads and requests via *parallel KV compaction*. Rather than performing memory management operations sequentially on CPU for each head and request, parallel KV compaction optimizes memory allocation and recycling by packing fragmented free memory lists into contiguous regions directly on the GPU in parallel. Parallel KV compaction is supported by three key on-GPU data structures:

**1. Unified Pages.** GPU memory is divided into fixed-size pages containing vectors stored at various precisions. Each page is dynamically parsed according to the precision requirements of the head and request, while an attention GPU kernel is co-designed with the page layout to maximize memory bandwidth utilization.

**2. Circular Free Page List.** All page IDs are managed in a centralized, GPU-resident circular list. Both free and used pages are kept in contiguous regions, enabling efficient page allocation and recycling via parallel prefix sum.

**3. Bidirectional Page Table.** Instead of maintaining separate page tables for high- and low-precision pages, LeanKV consolidates both into a single bi-directional page table to minimize metadata overhead. High precision page IDs grow from the left side of the table, and low-precision page IDs grow from the right side.

We implement LeanKV on vLLM [32], a state-of-the-art LLM inference system, and evaluate it across three prominent model families including the emerging thinking model. The evaluation is conducted on representative workloads that demand advanced reasoning capabilities, such as mathematics and coding. Our experimental results demonstrate that LeanKV offers a superior cost-accuracy tradeoff compared to existing KV cache management methods. Specifically,

LeanKV compresses the KV cache by  $2.7\times$  to  $5.7\times$  with near-lossless accuracy, resulting in throughput improvement of  $1.9\times$  to  $5.4\times$ . The throughput improvement is primarily enabled by the parallel KV compaction mechanism, which reduces management overhead by three orders of magnitude, decreasing the proportion of memory management time in total execution latency from up to 76% to less than 1% compared to a sequential CPU-based implementation.

## 2 Background and Related Work

In this section, we describe Transformer-based large language models and review existing techniques for KV cache management aimed at improving LLM serving efficiency.

### 2.1 Large Language Models

**Transformer Architecture.** Large language models (LLMs) are predominantly built upon the Transformer architecture [61], which is used to capture complex long-range dependencies in sequential data. At the core of Transformer architecture is the attention mechanism, which allows each token in a sequence to weigh the significance of other tokens when constructing its contextualized representation. Mathematically, the attention computation is defined as:

$$\begin{aligned} \text{Attention}(\mathbf{Q}, \mathbf{K}, \mathbf{V})_i &= \sum_{j=1}^i \text{softmax} \left( \frac{\mathbf{Q}\mathbf{K}^\top}{\sqrt{d}} \right)_{ij} \mathbf{v}_j \\ &= \sum_{j=1}^i \frac{\exp \left( \frac{\mathbf{q}_i \cdot \mathbf{k}_j}{\sqrt{d}} \right)}{\sum_{n=1}^i \exp \left( \frac{\mathbf{q}_i \cdot \mathbf{k}_n}{\sqrt{d}} \right)} \mathbf{v}_j \end{aligned} \quad (1)$$

**Q** and **K** are matrices of size  $l \times d$ , representing the queries and keys, respectively, where  $l$  denotes the number of tokens and  $d$  represents the feature dimensionality. Vectors  $\mathbf{q}_i$ ,  $\mathbf{k}_i$ , and  $\mathbf{v}_i$  correspond to the query, key, and value of the  $i^{\text{th}}$  token. The dot product between **Q** and **K** measures the relevance between each pair of query and key. The softmax function normalizes these dot products to form a probability distribution, referred to as attention scores, which are used to compute a weighted sum of the value vectors and produce the output.

To capture a broader range of interactions between tokens, Transformer models employ multi-head attention (MHA), where each head independently computes attention using distinct projections of queries, keys, and values. The outputs from different heads are concatenated and linearly transformed to create a more expressive representation. Grouped-query attention (GQA) [5] improves the efficiency of MHA by allowing a group of query heads to share the same projection of keys and values, referred to as a KV head.

**Autoregressive Generation and KV Cache.** The autoregressive generation process of LLMs consists of two phases: the *prompt phase*, during which the model computes latent representations for all tokens in the *prompt*, the user-provided

context, and generates the first new token, and the *generation phase*, where the model iteratively generates subsequent tokens by attending to both the prompt and previously generated tokens. To avoid redundant computations across generation steps, *KV cache* is introduced to store the keys and values of all previous tokens. However, the size of the KV cache grows linearly with both the sequence length and batch size, quickly becoming a bottleneck for inference throughput [32, 67]. Therefore, efficient KV cache management is critical for alleviating memory bottlenecks and improving LLM serving efficiency.

## 2.2 KV Cache Optimization

**PagedAttention.** Static KV cache management systems [1, 67] reserve memory for the maximum possible sequence length, leading to considerable memory waste when actual sequences are shorter. To mitigate this inefficiency, vLLM [32] introduces *PagedAttention*, which partitions the KV cache into pages, each containing a fixed number of tokens, and allocates the pages on-demand as the sequence length grows. By managing the KV cache at the granularity of pages, vLLM reduces memory waste and enables larger batch sizes to improve serving efficiency.

**KV Cache Quantization.** Quantization [16, 22, 27, 43] reduce the KV cache size by approximating high-precision floating points with discrete low-bit values. To quantize a given tensor  $\mathbf{X}$ , we first calculate the scale  $s$  and zero point  $z$  as shown in Eq. (2), where  $\mathbf{X}_{\max}$  and  $\mathbf{X}_{\min}$  represent the maximum and minimum values in  $\mathbf{X}$ , and  $b$  is the bit-width. Then, quantization is applied element-wise as:  $\mathbf{Q} = \text{round}\left(\frac{\mathbf{X} + z}{s}\right)$ . During inference, the original values are approximately reconstructed via dequantization:  $\hat{\mathbf{X}} = s \cdot \mathbf{Q} - z$ . Unlike the quantized tensor  $\mathbf{Q}$ , the metadata  $s$  and  $z$  are kept in higher precision (e.g., FP16) to ensure more accurate dequantization.

$$s = \frac{\mathbf{X}_{\max} - \mathbf{X}_{\min}}{2^b - 1}, \quad z = -\mathbf{X}_{\min} \quad (2)$$

State-of-the-art KV cache quantization methods such as Atom [70] and Qserve [37] apply this process to each key and value vector independently. However, these uniform quantization methods, which apply a fixed bit-width across keys and values of all tokens, may not be optimal. They overlook the varying importance of tokens as well as the different roles of keys and values in the attention calculation.

**KV Cache Pruning.** Several recent works [10, 20, 35, 40, 64, 69] have explored KV cache pruning to alleviate the memory bottleneck in LLM inference, which can be considered as an extreme case of quantization. These methods use attention scores to assess token importance and evict less important tokens, thereby reducing the KV cache size. The effectiveness of these methods, however, is limited by their static and inflexible allocation of memory resources. Specifically, H2O [69] and SnapKV [35] allocate the same memory budget uniformly

across all attention heads and layers. PyramidKV [10] allocates more memory in lower layers and less in higher ones, based on the empirical observation that the number of important tokens shrinks as the model depth increases, but still relies on static heuristics and cannot dynamically adjust cache allocations to suit various workloads. Complementary to KV cache pruning, another line of work [33, 52] addresses GPU memory constraints by offloading the entire KV cache to CPU memory and selectively loading important tokens to the GPU for attention computations. However, these methods do not inherently reduce the KV cache size and incur significant latency due to data transfers between the CPU and GPU.

## 3 The Case for Differentiated KV

We present the case for three levels of differentiation within the KV cache, motivating the design of LeanKV.

### 3.1 Differentiated Impacts of Keys and Values

While the significance of different tokens can be directly inferred from attention scores, the roles of the key and value vectors within a token are less obvious. However, examining Equation 1 reveals a divergence in their impacts. Each token’s contribution to the attention output depends on two factors: the attention score from softmax and the value vector. Key vectors, as part of the shared softmax denominator, influence the attention scores of all tokens, whereas value vectors only affect their respective token’s contribution to the output.

Beyond the broader impact of key vectors, it is crucial to establish the *relative significance* of attention scores, determined by key vectors, over value vectors. Without this, the significance of key vectors could be overshadowed by that of value vectors. To this end, we reformulate the attention mechanism as a weighted sum of unit vectors, as presented in Equation 3. This formulation decomposes each input token’s contribution into two components: the unit vector  $\frac{\mathbf{v}_j}{\|\mathbf{v}_j\|}$ , representing only the direction of the token in feature space, and a coefficient, defined as the product of the attention score and the norm of the value vector, which determines the relative significance of the token’s direction. This allows us to assess the relative importance of attention scores and value vectors by examining their contributions to these coefficients.

$$\text{Attn}(\mathbf{Q}, \mathbf{K}, \mathbf{V})_i = \sum_{j=1}^i \underbrace{\text{softmax}\left(\frac{\mathbf{Q}\mathbf{K}^\top}{\sqrt{d}}\right)_{ij}}_{\text{Coefficient}} \|\mathbf{v}_j\| \underbrace{\frac{\mathbf{v}_j}{\|\mathbf{v}_j\|}}_{\text{Unit vector}} \quad (3)$$

Figure 1 presents the distributions of the average attention score per token and the norms of value vectors across three representative layers of the Llama3-8B model [17], evaluated on the first one thousand articles from the WikiText dataset [42]. Notably, the attention scores span seven orders of magnitude, vastly exceeding the range of value vector norms,

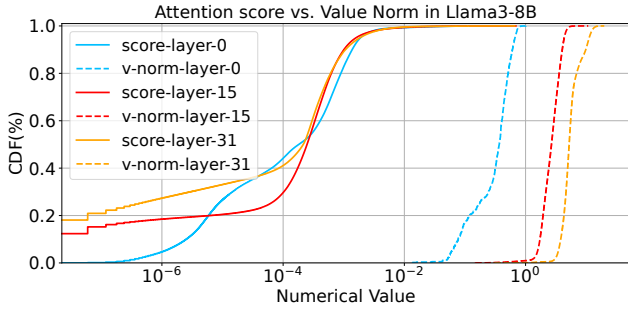


Figure 1: Distribution of attention score and value vector norm in Llama3-8B.

which only cover at most two orders of magnitude. Similar patterns are also observed in the larger Llama3-70B model. This pronounced disparity highlights the pivotal role of attention scores in determining each token’s contribution to the attention output. We therefore conclude that key vectors exert a broader and more impactful influence than value vectors, motivating further exploration of processing key and value vectors at distinct precision levels.

### 3.2 Differentiated Token Importance

Tokens contribute to attention outputs with varying degrees of importance, as reflected by their attention scores. By exploiting these differences, we can apply finer-grained compression strategies that go beyond uniformly quantizing all tokens [37, 70] or exclusively pruning the least important ones [10, 69]. Specifically, we store progressively less important tokens at decreasing precision levels, ultimately leading to the pruning of the least important tokens.

To investigate the feasibility of this hierarchical approach, we experiment with a simple design: quantizing both the key and value vectors of significant tokens to 8 bits while pruning insignificant ones. Figure 2 compares the performance of the FP16 baseline, 8-bit quantization, pruning, and the combination of 8-bit quantization with pruning on the general knowledge question answering benchmark MMLU [26] using the Llama3-8B model. For both pruning and the combined approach, approximately 50% of insignificant tokens are pruned. The resulting accuracy is nearly indistinguishable among the four approaches. However, the combination of 8-bit quantization and pruning achieves the lowest memory usage. The improved efficiency of this combined approach motivates us to further explore the spectrum of KV cache compression by introducing varying levels of precision to accommodate tokens of differing significance.

### 3.3 Dynamic Sparsity Patterns

Existing approaches to KV cache pruning primarily rely on static memory allocation for each transformer layer in LLMs, either distributing memory uniformly [20, 35, 64, 69] or al-

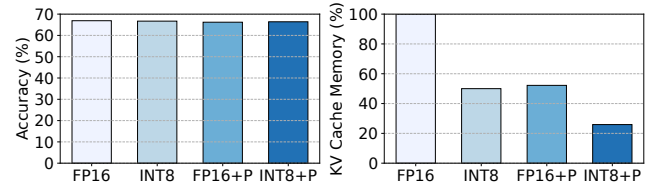


Figure 2: Accuracy and normalized KV cache memory usage of the Llama3-8B model on MMLU

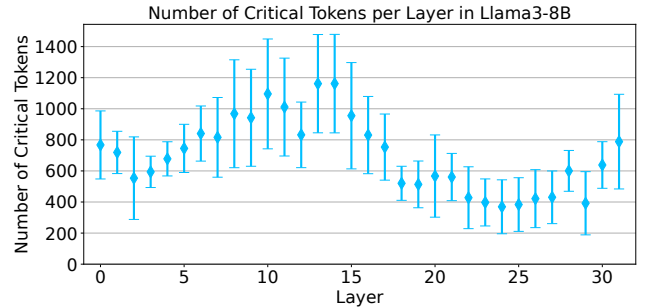


Figure 3: Number of critical tokens per layer in Llama3-8B to preserve 95% of the total attention score.

locating it based on offline profiling [10]. However, LLMs exhibit dynamic sparsity patterns that vary across both attention heads and requests, which static memory allocation cannot adequately handle. To evaluate the sparsity of attention computation, we analyze the minimum number of critical tokens required to retain the majority of information, specifically by preserving a target percentage (e.g., 95%) of the total attention score.

We begin by investigating dynamic sparsity patterns across layers. Using the first thousand articles from the Wikitext dataset, we evaluate the Llama3-8B model. Figure 3 illustrates the average number of critical tokens per layer, aggregated across all KV heads, required to retain 95% of the total attention score. Vertical bars represent the standard deviation, capturing variability across individual requests. Notably, the degree of sparsity varies considerably across layers, as indicated by differences in the number of critical tokens.

Next, we delve into the dynamic sparsity within individual layers. Figure 4 presents the average number of critical tokens per KV head for three representative layers, with horizontal bars indicating the standard deviation across requests. The sparsity pattern remains highly dynamic: within each layer, the number of critical tokens varies significantly across KV heads. Furthermore, within individual KV heads, the number of critical tokens can vary substantially across requests, as shown by the high standard deviation in some KV heads.

These highly dynamic sparsity patterns, across layers, attention heads, and individual requests, underscore the necessity of adaptive memory management on a per-head and per-request basis.

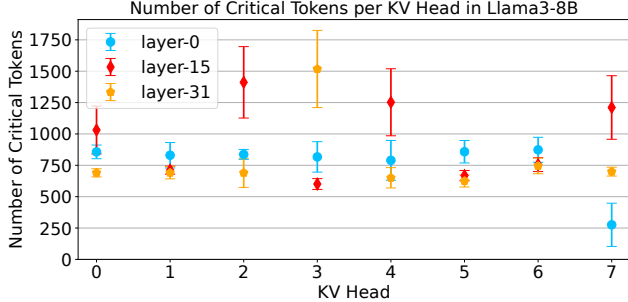


Figure 4: Number of critical tokens per KV head in Llama3-8B to preserve 95% of the total attention score.

### 3.4 Key Findings and Implications

Our findings reveal three critical levels of differentiation within the KV cache:

- Keys exert a broader impact on attention computation than values, motivating differentiated precisions for keys and values.
- Tokens vary in importance as reflected by their attention scores, motivating a fine-grained, hierarchical compression strategy.
- Attention sparsity patterns vary across requests and attention heads, requiring dynamically managing memory resources on a per-request and per-head basis.

Collectively, these insights guide the design of LeanKV, which integrates differentiated precision assignments for keys and values, hierarchical token importance handling, and per-request and per-head memory management.

## 4 KV Compression Policy

We present the KV compression policy of LeanKV that addresses the three levels of differentiation within the KV cache. First, to reflect the greater impact of keys on attention computation than values, we propose quantizing keys at a higher precision than values. For example, keys and values can be quantized to 8 and 4 bits (K8V4), or 4 and 2 bits (K4V2). Second, to account for the varying importance of tokens, we introduce a hierarchical compression strategy that classifies tokens into three significance levels: the most important tokens are quantized at high precision (e.g., K8V4), moderately important tokens at lower precision (e.g., K4V2), and the least important tokens are pruned. Finally, to address the dynamic sparsity patterns across requests and attention heads, we propose an adaptive memory management approach. Rather than imposing a fixed memory budget, our approach allows each attention head to determine its memory requirements dynamically based on its specific sparsity pattern.

Next, we describe the KV compression policy in greater detail, addressing the prompt phase and the generation phase separately. In both phases, compression is applied per-request and per-head, ensuring that memory usage is tailored to the specific sparsity pattern of each request and attention head.

**Prompt Phase.** In the prompt phase, key and value vectors for all tokens in the prompt are computed. The compression policy then determines the appropriate precision for storing each token based on its significance. The significance of the  $i^{th}$  token is calculated by averaging the  $N - i$  attention scores it receives from subsequent tokens, where  $N$  denotes the sequence length. In the case of GQA and MHA, scores from all attention heads associated with the KV head are aggregated using the maximum operation. To mitigate premature compression, the most recent  $W$  tokens are always quantized at high precision, where  $W$  is typically set to 64. For the remaining tokens, the policy determines the precision level of the  $i^{th}$  token by comparing its significance score to the theoretical average  $\frac{1}{i}$ , based on the intuition that tokens with scores below average are less critical. Specifically, the  $i^{th}$  token is quantized at high precision if its significance score exceeds  $\frac{\alpha_h}{i}$ , at low precision if its score lies within the interval  $[\frac{\alpha_l}{i}, \frac{\alpha_h}{i}]$ , and is pruned otherwise. The parameters  $\alpha_l$  and  $\alpha_h$ , which define the thresholds for high- and low-precision quantization, are determined offline through profiling on a calibration dataset. As a result of this hierarchical compression, the KV cache is conceptually divided into two parts: a high-precision section  $KV_h$  and a low-precision section  $KV_l$ .

**Generation Phase.** In the generation phase, a single token is compressed at each step, aligning with the autoregressive nature of the generation process. The most recent token is added to the recent window to prevent premature compression, while the earliest token  $t_c$  in the window becomes a candidate for more aggressive compression. The compression procedure can be divided into two parts. First, token  $t_c$  is quantized at either a high or low precision and added to the corresponding section of the KV cache, or it may be completely pruned. Next, if  $t_c$  is quantized, the least significant token  $t_v$  in the corresponding precision section of the KV cache is either re-quantized to lower precision or pruned, depending on its significance. Essentially, this policy establishes a smooth downgrading path for the less important token: rather than being pruned directly, it is first re-quantized to low precision, with pruning occurring only if it remains insignificant.

The detailed procedure is outlined in Algorithm 1, following the same intuition and parameters as the prompt phase. Given the sequence length  $N$ ,  $t_c$  is quantized at high precision and added to  $KV_h$ , the high precision KV cache (line 6), if its significance exceeds  $\frac{\alpha_h}{N}$ . Subsequently, the least significant token in  $KV_h$  is identified as the victim token  $t_v$  for more aggressive compression (line 7). If  $t_v$ 's significance exceeds  $\frac{\alpha_h}{N}$ , it remains in  $KV_h$ ; if it falls within  $[\frac{\alpha_l}{N}, \frac{\alpha_h}{N}]$ ,  $t_v$  is re-quantized to low precision and moved to  $KV_l$ , the low precision KV cache (line 9); otherwise,  $t_v$  is pruned. Similarly, if  $t_c$ 's significance lies within  $[\frac{\alpha_l}{N}, \frac{\alpha_h}{N}]$ , it is quantized to low precision and added to  $KV_l$  (line 14). The least important token in  $KV_l$  is designated as the victim  $t_v$  (line 15), and is further pruned if its significance falls below  $\frac{\alpha_l}{N}$  (line 17).

**Discussion.** The proposed KV compression policy is highly

extensible, allowing for the potential use of more than three precision levels. We adopt three precision levels primarily to minimize metadata overhead and improve system efficiency, as will be detailed in the following section. Additionally, we use a shared set of thresholds for all attention heads, as our empirical studies demonstrate that this approach is sufficient to capture the varying sparsity patterns across different heads. Notably, LeanKV can efficiently support more flexible compression policies, such as tuning thresholds for each head individually, which could potentially further optimize the balance between model accuracy and memory efficiency. We leave the exploration of such flexible policies for future work.

---

**Algorithm 1:** KV compression policy (generation)

---

```

1: Input: Parameters  $\alpha_h, \alpha_l$ ; High & low precision  $P_h$  &  $P_l$ 
2: Input: Candidate token  $t_c$ ; Sequence length  $N$ 
3: Input: High & low precision KV cache  $KV_h$  &  $KV_l$ 
4: Function: Significance Score; Quantization Quant;
5: if  $\text{Score}(t_c) \geq \frac{\alpha_h}{N}$  then
6:    $KV_h.\text{add}(\text{Quant}(t_c, P_h))$ 
7:    $t_v = \text{argmin}_{t \in KV_h}(\text{Score}(t))$ 
8:   if  $T_l \leq \text{Score}(t_v) < T_h$  then
9:      $KV_h.\text{remove}(t_v)$ ,  $KV_l.\text{add}(\text{Quant}(t_v, P_l))$ 
10:  else if  $\text{Score}(t_v) < T_l$  then
11:     $KV_h.\text{remove}(t_v)$ 
12:  end if
13: else if  $\text{Score}(t_c) \geq \frac{\alpha_l}{N}$  then
14:    $KV_l.\text{add}(\text{Quant}(t_c, P_l))$ 
15:    $t_v = \text{argmin}_{t \in KV_l}(\text{Score}(t))$ 
16:   if  $\text{Score}(t_v) < T_l$  then
17:      $KV_l.\text{remove}(t_v)$ 
18:   end if
19: end if

```

---

## 5 Memory Management

In this section, we describe LeanKV’s memory management mechanism which efficiently supports the three levels of differentiation in the KV cache. We first highlight the challenges posed by these differentiations in memory management, and then present parallel KV compaction, a novel memory management technique that effectively tackles the challenges.

### 5.1 Challenges

**The Need for Flexible Paging.** In PagedAttention [32], all tokens are stored at the same precision, allowing for a fixed page format. However, the differentiation of key and value vectors, along with varying token importance, introduces multiple precision levels both within individual tokens and across different tokens, making a fixed page format insufficient. Specifically, a fixed page format requires conservatively allocating high-precision slots for all tokens regardless of their actual precisions, leading to considerable memory wastage. Suppose

memory is allocated to accommodate the highest precision K8V4, a token with K4V2 precision would waste 50% of the memory. Worse, such a fixed page format results in misaligned memory accesses, which hinder memory bandwidth utilization and reduce overall computational efficiency.

**Substantial KV Compaction Overhead.** In PagedAttention, memory management complexity is  $O(\#requests)$ , as memory is partitioned uniformly across attention heads, with identical page IDs assigned to each head. In contrast, LeanKV must handle varying numbers of high- and low-precision tokens across different heads, mapping these irregular memory requirements to physical memory. We term this process *KV compaction*, whose complexity is  $O(\#requests \times \#heads)$ , significantly higher than that of PagedAttention. If KV compaction were performed sequentially on CPUs, its overhead could overshadow the performance gains from KV cache compression. Moreover, to track both high-precision and low-precision tokens, a straightforward approach would involve using separate data structures for each precision, resulting in increased metadata overhead.

### 5.2 Parallel KV Compaction

A detailed analysis of the KV compaction process reveals opportunities for parallelization and performance optimization. KV compaction can be divided into two phases: *planning* and *coordination*. In the planning phase, each head independently determines its memory allocation requirements. The subsequent coordination phase synchronizes these per-head requirements and maps them to the GPU’s physical memory. For instance, consider two attention heads require 16 and 32 bytes, respectively, as determined in the planning phase, with all GPU physical memory available. Then in the coordination phase, physical memory bytes 0 to 15 are allocated to the first head, and bytes 16 to 48 to the second. The primary source of increased memory management complexity lies in the planning phase, which is perfectly parallel and well-suited to the GPU’s parallel compute capabilities. Parallelizing the coordination phase is more challenging, as it requires synchronization across heads. However, we observe that this phase can be parallelized effectively via parallel prefix sum [44], provided that the free memory region is contiguous.

Thus, we propose *parallel KV compaction*, a novel management technique that efficiently performs per-head dynamic memory allocation and recycling in parallel directly on the GPU. Parallel KV compaction is enabled by three GPU-resident data structures collectively: the (1) *unified pages* to enable flexible paging, (2) the *circular free page list* to efficiently parallelize memory management, and (3) the *bidirectional page table* to minimize metadata overhead for tracking tokens of differentiated precisions.

**Unified Pages.** *Unified pages* abstract away the complexity of differentiated precisions both within individual tokens and across different tokens, thereby simplifying the implementation of parallel KV compaction. Specifically, we partition

the available GPU memory into evenly sized pages, each configured *upon allocation* to store tokens at a given precision. Each unified page is organized into six segments: quantized keys, quantization metadata for keys, quantized values, quantization metadata for values, token scores, and positions. The quantization metadata includes scales and zero points for the key and value vectors. The number of tokens stored per page is adjusted according to the quantization configuration, ensuring compact memory usage. Furthermore, by consolidating keys, values, and their metadata into a single structure, unified pages enhance data locality and eliminate the need for scattered lookups, improving memory access efficiency during attention computation.

**Circular Free Page List.** The *circular free page list* serves as the cornerstone of parallel KV compaction, facilitating the parallelization of memory allocation and recycling by maintaining both free and used pages in contiguous regions.

This centralized, GPU-resident data structure contains all Page IDs and tracks free pages through a pair of pointers: a start pointer for allocations and an end pointer for recycling. These pointers wrap around to the beginning of the list upon reaching the end, forming a circular structure. When a page is allocated, the start pointer advances to the next available Page ID; when a page is freed, the end pointer advances to add the released Page ID back into the list. Both the available and unavailable regions in the list remain contiguous, enabling the coordination phase in memory management to be parallelized via parallel prefix sum.

In parallel KV compaction, after each head determines the number of pages to be allocated or freed, a parallel prefix sum operation computes a unique offset for each head relative to the start or end pointer, ensuring non-conflicting operations within the list. For memory allocation, each head concurrently retrieves its new page IDs from its designated region in the list, with the start pointer incremented by the cumulative number of pages required across all heads. Similarly, for memory recycling, each head concurrently writes freed page IDs to its designated region, with the end pointer incremented by the total number of pages released.

**Bidirectional Page Table.** Similar to PagedAttention, LeanKV maintains a page table for each attention head, mapping each request to its corresponding list of page IDs. To avoid the doubled metadata overhead associated with maintaining separate page tables for high- and low-precision pages, LeanKV introduces a unified, GPU-resident data structure called the *bidirectional page table*. This structure efficiently supports the use of three precision levels for KV cache, as proposed in Section 4, minimizing the metadata overhead. In each entry of the bidirectional page table, high-precision page IDs grow from the left side of the list, while low-precision page IDs grow from the right, dynamically adapting to the precision requirements of the workload. The length of each page table entry is determined by the maximum sequence length divided by the tokens per high-precision page, ensuring no

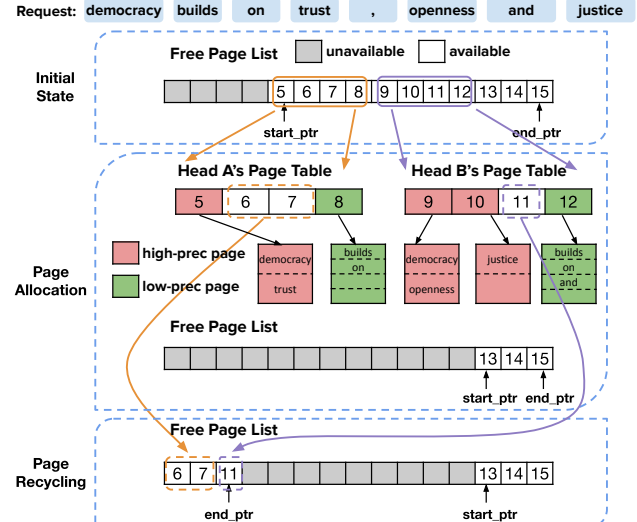


Figure 5: Memory management flow in the prompt phase.

overflow since low-precision pages always contain more tokens than high-precision ones. This unified approach not only minimizes metadata overhead but also eliminates the need for separate lookups based on precision levels, thereby enhancing memory access efficiency during attention computations. The memory overhead of the bidirectional page table is minimal: for example, with a batch size of 128 on Llama-2-7B, which has 32 layers and 32 attention heads per layer, the total size of all bidirectional page tables is only 64 MB. By contrast, the KV cache for a single request occupies 2 GB.

### 5.3 KV Compaction Workflow

We delve into the KV compaction workflow during the prompt and generation phases, illustrating how the three data structures interact to enable differentiated KV cache compression. Notably, KV compaction is executed once per inference step for all requests in the batch and all layers in the LLM. This design ensures sufficient parallelism for efficient GPU execution of parallel KV compaction, while amortizing the associated GPU kernel launch overheads.

**Prompt Phase.** Figure 5 illustrates the KV compaction workflow during the prompt phase using an example request with eight tokens. In this setting, one high-precision page can store two tokens, and one low-precision page can store four. Since the exact number of high- and low-precision pages required by each head is unknown prior to running the compression algorithm, we conservatively allocate four unified pages per head, assuming that all tokens will be stored at high precision. Each head then independently applies the KV cache compression algorithm to determine which tokens to store at high-precision, low-precision, or to prune. This step constitutes the *planning phase*, during which each head calculates its specific memory needs based on its unique sparsity pattern. In this example, the first head uses one high-precision page, while the second

head uses two; both heads also require one low-precision page. High-precision pages are allocated from the left side of the bidirectional page table, while low-precision pages are allocated from the right side. Following the planning phase, any unused pages are marked for recycling, triggering the *coordination phase*. Here, we employ a parallel prefix-sum-based approach, as described in the previous section, to facilitate efficient and conflict-free page recycling across heads.

**Generation Phase.** At each generation step, a head allocates a new page only if either its high-precision or low-precision pages are full, requiring at most one additional page per step. Each head independently checks its page availability and, if needed, allocates a new page in parallel using the prefix-sum-based approach. Unlike in the prompt phase, page recycling is not performed during generation, as the total number of stored tokens either remains the same if an old token is evicted or increases by one if no eviction occurs. Once a request is finished, all pages allocated for that request are recycled, freeing up memory for incoming requests.

## 6 Implementation

We implement LeanKV on top of vLLM, comprising 4.5K lines of CUDA/C++ code and 9K lines of Python. We first outline the architecture of LeanKV and then detail our custom GPU attention kernel, designed to efficiently support the differentiated KV cache compression.

### 6.1 LeanKV Architecture

The architecture of LeanKV is illustrated in Figure 6. At each inference step, the scheduler batches as many requests as possible within the available GPU memory to maximize throughput, sending the selected requests to all workers. Each GPU hosts one worker, responsible for executing a segment of the model. LeanKV utilizes tensor parallelism [54], where each worker handles a partition of each matrix multiplication and a subset of the attention heads. Each worker includes a dedicated memory manager to oversee the KV cache for its assigned attention heads, using the method described in Section 5. Due to dynamic sparsity patterns, memory requirements vary per head for each request, leading to an irregular memory layout. Additionally, each worker incorporates an execution engine for model computation. To support differentiated KV cache compression, the execution engine integrates a KV compressor and a custom GPU attention kernel. After computing key and value vectors, the KV compressor is invoked to compress them following the policy described in Section 4, storing the results in the KV cache. The custom GPU attention kernel then efficiently computes the attention output using the compressed KV cache.

### 6.2 Efficient Attention Kernel

We develop a custom GPU attention kernel that efficiently supports differentiated KV cache compression, fully harness-

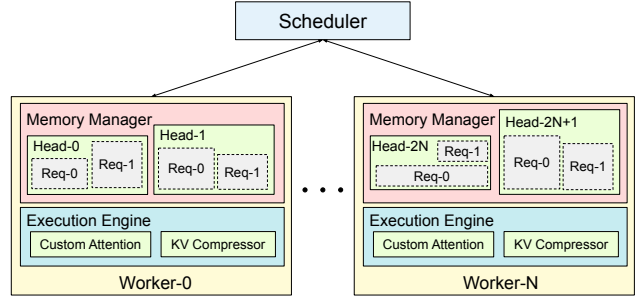


Figure 6: LeanKV architecture.

ing the reduction in memory access volume and translating it into accelerated performance.

Overall, we assign each CUDA thread block to process a single attention head per sequence. However, mixed-precision quantization introduces potential load imbalance, as high-precision tokens demand more bandwidth, which is the bottleneck of attention, than low-precision ones. Thanks to unified pages that store tokens of the same precision together, we mitigate this issue by having thread warps iterate over high-precision pages first, followed by low-precision pages, ensuring that threads within a warp remain load-balanced. Each page is processed in two phases: dot product between the query and keys to derive attention scores, and weighted sum of values. These two phases follow different computation patterns: reduction over the feature dimension and token dimension, respectively. To ensure coalesced and vectorized memory accesses for both phases, we design tailored data layouts and parallelization strategies, elaborated as follows.

For key processing, each warp handles one page at a time, with threads in the warp divided into groups responsible for distinct keys. Within a group, each thread fetches its assigned keys in a vectorized manner, performs dequantization on the fly, and computes a partial dot product between the keys and corresponding query. Using a straightforward layout such as  $[F, N_{\text{tokens}}]$  for keys in each page, where  $F$  denotes the feature dimension length, would cause threads within a group to fetch non-contiguous elements strided by  $N_{\text{tokens}}$  when parallelizing across the feature dimension. Alternatively, using  $[N_{\text{tokens}}, F]$  would cause thread groups to fetch non-contiguous elements strided by  $F$  when parallelizing across tokens. Both layouts suffer inefficient strided memory accesses, leading to low bandwidth utilization. Instead, we organize the layout of keys as  $[\frac{F}{K_{\text{vec}} \times K_{\text{group}}}, N_{\text{tokens}}, K_{\text{group}}, K_{\text{vec}}]$ , where  $K_{\text{vec}}$  denotes the vectorization factor and  $K_{\text{group}}$  denotes the number of threads per group. During each execution step, each thread fetches  $K_{\text{vec}}$  consecutive elements, threads within a group collectively fetch  $K_{\text{group}}$  adjacent chunks, and groups within the warp access contiguous chunks along the  $N_{\text{tokens}}$  dimension. As a result, the combined memory accesses of all threads in a warp are contiguous, enabling memory coalescing and maximizing bandwidth utilization.

For value processing, tokens in a page are evenly distributed

across thread groups in a warp; within each group, individual threads perform sum reductions over specific ranges of the feature dimension and save their accumulation results in registers. Once all groups finish, a tree reduction aggregates these partial results and produces the output. The number of registers required per thread is proportional to the feature dimension range assigned to it, while during key processing each thread only requires a single register to store the partial dot product. As a consequence, vectorization along the feature dimension, as used in key processing, is not suitable for value processing, because it would significantly increase register pressure by forcing each thread to handle a larger portion of the feature dimension. To better align with the computation pattern of reduction across tokens during value processing, we apply vectorization to the token dimension instead, which reduces register pressure and ensures more effective parallelization. We organize the layout of values as  $[\frac{F}{V_{\text{group}}}, \frac{N_{\text{tokens}}}{V_{\text{vec}}}, V_{\text{group}}, V_{\text{vec}}]$  accordingly.

## 7 Evaluation

We first evaluate the effectiveness of LeanKV’s differentiated KV cache compression policy and analyze the sensitivity of different models to KV cache compression. Next, we evaluate the efficiency of the memory manager as well as the end-to-end throughput improvements achieved by LeanKV.

### 7.1 Experiment Setup

We evaluate LeanKV on five models spanning three major families: Llama3-8B and 70B [60], Qwen2.5-7B and 32B [28], and the recently released thinking model QwQ-32B [58], which generates extended chains of thought and exhibits strong performance on complex reasoning tasks. Our evaluation covers a diverse set of mainstream benchmarks across multiple task domains, including general knowledge (MMLU [26] and MMLU-Pro [55]), mathematics (GSM8K [13] and MATH [34]), code generation (HumanEval+ [11, 39] and MBPP+ [7, 39]), and long-context understanding (LongBench [8]). In addition, we assess LeanKV’s performance on QwQ-32B using two particularly challenging benchmarks: AIME24 [3], a high-school level mathematics competition dataset, and GPQA [48], which evaluates graduate-level science reasoning. Throughput and latency are measured on NVIDIA L40 GPUs, each equipped with 48 GB of memory [45].

### 7.2 Differentiated KV Compression Policy

We first assess the effectiveness of differentiated KV quantization and dynamic sparsity individually, and then evaluate the combined benefits of the proposed differentiated KV cache compression. To ensure the reliability of our results and mitigate the influence of noise and randomness inherent in floating-point computations, each experiment is repeated five

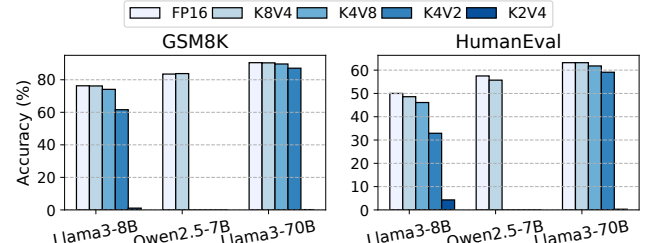


Figure 7: Performance of differentiated KV quantization.

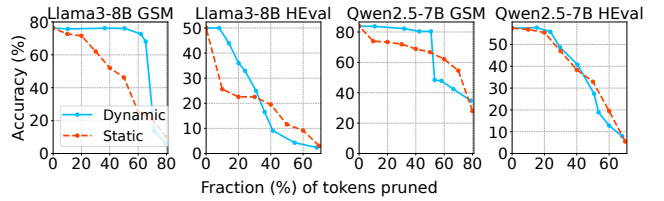


Figure 8: Performance of dynamic vs. static sparsity.

times with the dataset randomly shuffled, and the reported results represent the average across these runs.

**Evaluating Differentiated KV Quantization.** Figure 7 shows the performance of differentiated KV quantization on GSM8K and HumanEval+, namely K8V4 and K4V2, compared to FP16 baselines, across Llama-3 8B & 70B and Qwen-2.5 7B. To validate our intuition that keys have a more significant impact than values (Section 3.1), we additionally evaluate the mirror configurations, namely K4V8 and K2V4, where values are stored with higher precision than keys. Results show that K8V4 matches the accuracy of the FP16 baseline across all models and benchmarks. In contrast, its mirror configuration, K4V8, exhibits noticeable performance degradation, particularly for Qwen2.5-7B, where accuracy drops to nearly zero on both tasks. This pronounced sensitivity to 4-bit key quantization in Qwen2.5-7B is likely due to its GQA architecture, which applies aggressive KV compression with a queries-per-KV ratio of 7, substantially higher than the ratio of 4 used in Llama-3 8B. Similarly, K4V2 retains over 65% of FP16 accuracy across both benchmarks on Llama-3 8B and 70B, while the mirror configuration K2V4 results in near-zero accuracy. These results confirm that keys play a more critical role than values, and demonstrate the effectiveness of differentiated KV quantization in preserving accuracy while enabling aggressive compression.

**Evaluating Dynamic Sparsity.** We evaluate the effectiveness of per-head dynamic sparsity (Section 3.3) in identifying critical tokens, comparing it to the static sparsity method used in SnapKV [35] and H2O [69], which allocates an equal memory budget to all attention heads. Figure 8 reports results on Qwen2.5-7B and Llama3-8B across GSM8K and HumanEval+. The x-axis indicates the percentage of tokens pruned, while the y-axis shows the resulting task accuracy. Dynamic sparsity significantly outperforms static sparsity in Llama3-8B, maintaining full accuracy with 50% tokens pruned on GSM8K, and 10% tokens pruned for the more

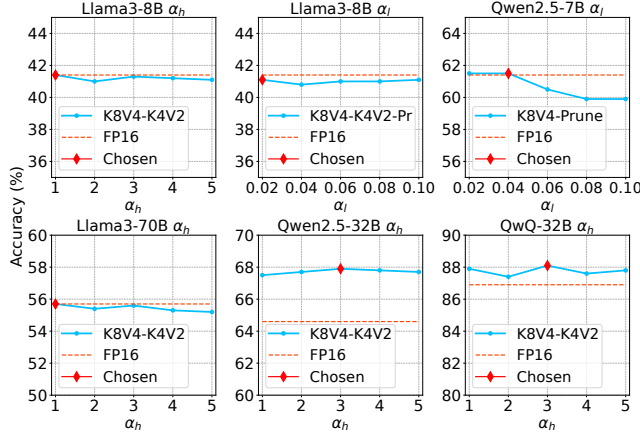


Figure 9: Calibrating the high- and low-precision threshold parameters  $\alpha_h$  and  $\alpha_l$  on the training split of the MATH dataset.

sensitive HumanEval+. For Qwen2.5-7B, dynamic sparsity also consistently surpasses static sparsity, achieving accuracy higher than 80% on GSM8k with 50% tokens pruned. While the improvement is less pronounced on HumanEval+, dynamic sparsity still yields higher accuracy at equivalent pruning ratios. In summary, per-head dynamic sparsity is superior to static sparsity by leveraging head-specific significance.

**Parameter Calibration.** As described in Section 4, LeanKV compares the significance score of a token with its theoretical average,  $\frac{1}{N}$ , where  $N$  denotes the sequence length. A token is quantized to high precision if its score exceeds  $\frac{\alpha_h}{N}$ , to low precision if its score falls within the interval  $[\frac{\alpha_l}{N}, \frac{\alpha_h}{N}]$ , and is pruned otherwise. To calibrate the appropriate parameters  $\alpha_h$  and  $\alpha_l$ , we utilize the training split of MATH [34]. We select MATH as the calibration dataset as it is comprised of complex mathematical reasoning tasks with high text information density, where even the removal of a single symbol can invalidate an argument. This makes MATH a highly suitable choice for parameter fitting, as the resulting compression parameters are expected to generalize well across other tasks. Additionally, MATH provides a dedicated training split, ensuring that parameter fitting does not involve testing data and mitigating potential overfitting.

We profile a consistent range of parameters across all evaluated models, as depicted in Figure 9. The x-axis represents the profiled parameter values, while the y-axis shows the resulting accuracy on the calibration dataset. Specifically, we profile  $\alpha_h$  within the integer range  $[1, 5]$ , progressively relaxing the high-precision threshold beyond the theoretical average. This adjustment accounts for aggregating scores from multiple attention heads by maximum for GQA, as mentioned in Section 4. The profiled values of  $\alpha_h$  achieve FP16-equivalent accuracy across all models, except for Qwen2.5-7B, which exhibits heightened sensitivity to 4-bit key quantization. Based on our profiling, we select the values of  $\alpha_h$  that yield the highest accuracy for each model:  $\alpha_h = 1$  for Llama-3 8B and 70B,  $\alpha_h = 3$  for Qwen2.5-32B and QwQ-32B, and  $\alpha_h = 0$

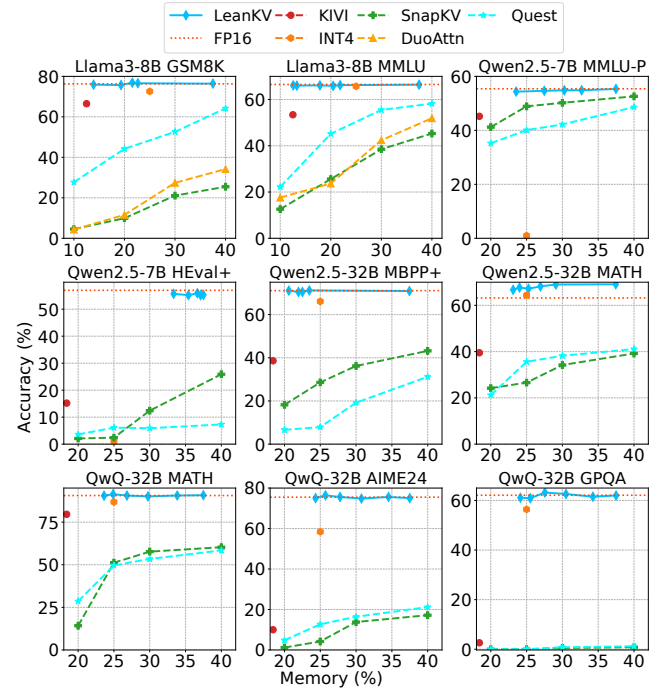


Figure 10: KV cache memory normalized to vLLM vs. benchmark performance tradeoff of LeanKV.

for Qwen2.5-7B. Subsequently, we profile the low-precision threshold  $\alpha_l$ , while keeping  $\alpha_h$  fixed. We observe that setting  $\alpha_l = 0.1$  induces at least 5% accuracy degradation on the larger models. As a result, we profile five equally spaced values within the range  $[0, 0.1]$  and select the one yielding the highest accuracy for each model. The final selected values of  $\alpha_l$  are 0.02 for Llama3-8B, 0.04 for Qwen2.5-7B, and 0 for the remaining models. While the profiled values cover a limited portion of the entire parameter space, as will be demonstrated in the following sections, LeanKV significantly outperforms existing baselines with these fitted parameters, highlighting its potential effectiveness.

**Evaluating Differentiated Compression Policy.** Finally, we evaluate the combined benefits of LeanKV’s KV cache compression policy. We compare LeanKV against several state-of-the-art baselines, including pruning-based methods such as H2O [69], SnapKV [35], and DuoAttention [63], quantization-based approaches such as 4-bit KV and KIVI [41], as well as KV partial loading techniques like Quest [56]. Table 1 summarizes the accuracy and KV cache memory usage of LeanKV normalized to vLLM [32] baseline, with the parameters tuned as described, for the evaluated non-thinking models. For the pruning-based baselines and Quest, we tune their memory usage to 50% of the baseline. LeanKV achieves near-lossless accuracy relative to the FP16 baseline, with an average degradation of only 0.3%, while using 19.3% to 36.7% memory. In contrast, all other baselines incur more significant accuracy degradation at comparable or higher memory usage. Further-

more, LeanKV dynamically adapts its memory usage based on the task’s information density. For example, LeanKV allocates less memory for the 5-shot MMLU benchmark compared to the 0-shot HumanEval+, where the prompt consists solely of the function name and comments.

LeanKV also outperforms baseline methods in long-context scenarios, as shown in Table 2, where we present results from one benchmark in each category of LongBench. For Llama3-8B and Qwen2.5-7B, LeanKV achieves memory usage of 14.9% and 27.0%, respectively, while baseline methods are tuned to 25% memory usage. Notably, LeanKV consistently achieves superior accuracy across all categories, with an average degradation of only 0.4%, while utilizing less or comparable memory compared to the baseline methods.

Furthermore, the performance gap between LeanKV and baseline methods becomes even more pronounced for the thinking model QwQ-32B on more challenging benchmarks, as demonstrated in Table 3. LeanKV matches the FP16 baseline performance using only 27.4% of the memory on average, while all other methods experience significant performance degradation. On the math competition benchmark AIME24, the most accurate baseline, 4-bit KV quantization incurs a 16.0% accuracy degradation. On the graduate-level science benchmark GPQA, the accuracy of pruning-based and KV partial loading methods drops to almost zero.

Lastly, Figure 10 depicts the performance-memory trade-offs of LeanKV across representative benchmarks under the profiled parameter values, namely  $\alpha_h \in [0, 5]$  (step size of 1) for all models and  $\alpha_l \in [0.02, 0.1]$  (step size of 0.02) for Llama3-8B and Qwen2.5-7B. We also include the accuracy of baseline methods within similar memory usage ranges for comparison. LeanKV consistently matches the FP16 baseline accuracy across different models and benchmarks within the profiled range of memory usage, demonstrating its robustness. In contrast, baseline methods experience significant accuracy degradation, particularly pruning-based and KV partial loading methods, which suffer rapid accuracy declines as memory usage decreases. In summary, LeanKV provides a superior performance-memory tradeoff compared to state-of-the-art methods.

### 7.3 System Performance

In this section, we provide a comprehensive evaluation of LeanKV’s performance, comparing it against state-of-the-art systems including vLLM, Quest, and SnapKV across various models. All experiments are conducted on a machine equipped with eight NVIDIA L40 GPUs. For models that fit within the memory of a single GPU, such as Llama3-8B and Qwen2.5-7B, we use one GPU. For larger models, we parallelize the computation across multiple GPUs: four GPUs for Llama3-70B, and two GPUs for Qwen2.5-32B and QwQ-32B. Our evaluation focuses on latency breakdown, attention kernel speedup, and end-to-end throughput to demonstrate the efficiency and scalability of LeanKV.

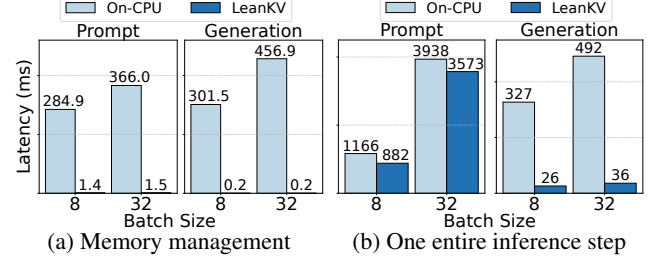


Figure 11: Latency comparison between parallel KV compaction and on-CPU multi-threaded memory management.

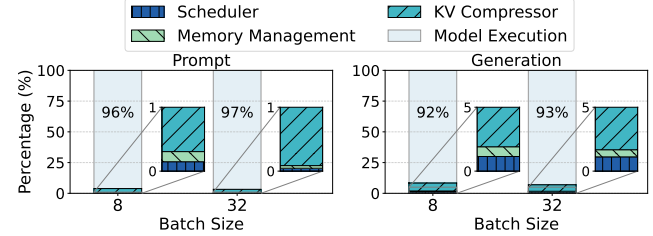


Figure 12: Latency breakdown of LeanKV.

**Memory Management Overhead.** Figure 11 compares LeanKV’s on-GPU parallel KV compaction with an alternative implementation that performs multi-threaded memory management on the CPU. Evaluated with a sequence length of 1024 tokens across different batch sizes, LeanKV reduces memory management latency by up to three orders of magnitude relative to the on-CPU approach. For one entire inference step, LeanKV significantly outperforms the on-CPU approach, particularly in the generation phase, where the memory management overhead on the CPU far exceeds the model execution time. Therefore, LeanKV’s on-GPU parallel memory management is essential for ensuring that the performance benefits of KV cache compression are fully realized without being overshadowed by memory management overhead.

Figure 12 further illustrates the latency breakdown of LeanKV during one inference step. The memory management overhead is remarkably low thanks to LeanKV’s on-GPU parallel KV compaction, contributing less than 0.2% of the total latency in the prompt phase and under 0.9% in the generation phase. Model execution dominates the latency in both phases, accounting for 96–97% of the latency in the prompt phase and 92–93% in the generation phase. Notably, as the batch size increases, the percentage of time spent on model execution rises slightly, reflecting the scalability of LeanKV.

**Attention Kernel Speedup.** Figure 13 shows the speedup of the LeanKV’s custom attention kernel against vLLM under different quantization configurations. LeanKV achieves a near-linear speedup proportional to the reduction in KV cache size. For example, with K8V8, which halves the KV cache size relative to FP16 datatype, the theoretical speedup is 2 $\times$ , and LeanKV achieves 1.7 $\times$ . The slight gap is primarily due to the overhead of accessing quantization metadata and performing dequantization. Additionally, LeanKV achieves greater speedups on longer sequences, indicating that its bandwidth

Table 1: Accuracy and memory usage of LeanKV and baseline methods across models and benchmarks. Numbers in parentheses represent memory usage normalized to FP16. The memory usage is 50% for SnapKV, Quest, H2O and DuoAttn, 25% for INT4, and 12.5% for KIVI due to 2-bit quantization.

Benchmarks	Llama3-8B				Qwen2.5-7B					Qwen2.5-32B				Llama3-70B		
	FP16	LeanKV	INT4	DuoAttn	FP16	LeanKV	Quest	SnapKV	KIVI	FP16	LeanKV	Quest	KIVI	FP16	LeanKV	H2O
<b>GSM8K</b>	76.3	75.7 (19.3%)	72.6	32.2	83.5	83.6 (26.8%)	76.7	66.7	72.2	90.4	90.2 (23.6%)	82.8	79.3	90.5	90.2 (21.6%)	52.4
<b>MATH</b>	28.1	27.9 (21.6%)	23.9	9.3	58.0	57.7 (32.3%)	41.7	45.1	39.5	63.2	67.2 (25.3%)	44.3	42.6	48.7	47.6 (21.3%)	26.6
<b>MMLU</b>	66.5	66.1 (17.8%)	65.2	42.4	75.1	74.7 (30.3%)	64.7	48.2	53.1	83.8	83.8 (23.1%)	68.5	70.5	81.0	80.9 (20.1%)	55.9
<b>MMLU-Pro</b>	41.5	41.0 (21.5%)	39.1	34.6	55.4	54.9 (30.2%)	51.6	49.7	45.2	67.8	67.4 (24.5%)	59.5	54.5	60.1	60.0 (21.5%)	46.5
<b>HumanEval+</b>	50.0	48.0 (27.6%)	45.1	4.8	57.5	55.9 (36.7%)	8.5	32.9	15.2	49.4	49.4 (26.2%)	11.0	15.3	71.3	71.5 (26.7%)	29.2
<b>MBPP+</b>	59.3	61.6 (17.6%)	58.8	35.6	64.3	62.8 (27.9%)	33.3	44.7	18.3	71.1	70.5 (21.8%)	35.2	38.6	68.6	69.7 (22.0%)	33.2

Table 2: Evaluating LeanKV on LongBench. LeanKV uses 14.9% memory for Llama3.1-8B and 27.0% for Qwen2.5-7B. For Quest and SnapKV, the memory usage is 25%.

		Qasper	HotpotQA	GovReport	TREC	PCount	Lcc
<b>Llama3.1-8B</b>	<b>FP16</b>	40.9	61.3	34.0	73.0	6.9	62.2
	<b>LeanKV</b>	42.8	61.3	32.9	73.0	7.2	61.9
	<b>Quest</b>	38.9	59.8	30.6	66.5	6.4	56.8
	<b>SnapKV</b>	39.2	59.6	30.1	65.9	6.2	57.2
<b>Qwen2.5-7B</b>	<b>FP16</b>	26.5	27.8	33.4	71.0	5.7	61.9
	<b>LeanKV</b>	26.4	28.2	32.2	70.0	5.3	62.3
	<b>Quest</b>	23.6	25.2	31.4	65.6	4.3	53.3
	<b>SnapKV</b>	22.6	25.5	30.8	64.6	4.5	52.6

Table 3: Evaluating LeanKV on QwQ-32B thinking model.

Benchmarks	FP16	LeanKV	INT4	Quest	KIVI	SnapKV
<b>MATH</b>	90.6	90.6 (26.8%)	87.3	63.3	80.6	65.4
<b>GPQA</b>	62.1	63.2 (27.6%)	57.8	1.2	2.6	0.8
<b>AIME24</b>	75.5	75.3 (27.8%)	64.3	23.3	10.0	19.2

optimization techniques become increasingly effective as the sequence length grows.

**End-to-End Throughput.** Figure 14 presents the end-to-end throughput and achieved batch sizes of LeanKV compared to vLLM, Quest, and SnapKV. The maximum generation length is set to 16K tokens for QwQ-32B, 8K for Qwen2.5-32B, and 4K for the other models. We evaluate on 1000 sequences sampled from the MATH dataset [34], which naturally elicits chain-of-thought reasoning and typically leads to long generations reaching the specified limit. Compression thresholds for LeanKV are adopted from Figure 9. Across all models, LeanKV consistently achieves higher throughput than prior systems. Notably, LeanKV achieves a remarkable 5.4× higher throughput over vLLM on the QwQ-32B thinking model, while Quest and SnapKV achieve only 1.6× and 1.8× speedups, respectively. This result highlights the superior efficiency of LeanKV in processing long sequences, making it particularly well-suited for tasks that require extended reasoning.

The throughput improvements are directly correlated with the larger batch sizes supported by LeanKV, enabled by its KV cache compression techniques. For instance, with the QwQ-32B model, LeanKV sustains a batch size of 15.9, far exceeding vLLM’s batch size of 2.7. The increased batch size enables LeanKV to maximize the utilization of GPU compute capacity, leading to higher throughput. In contrast, Quest supports the same batch size as vLLM because it retains

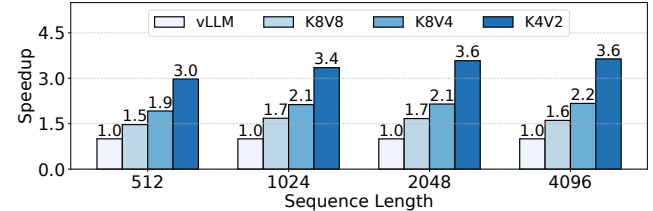


Figure 13: Attention kernel speedup.

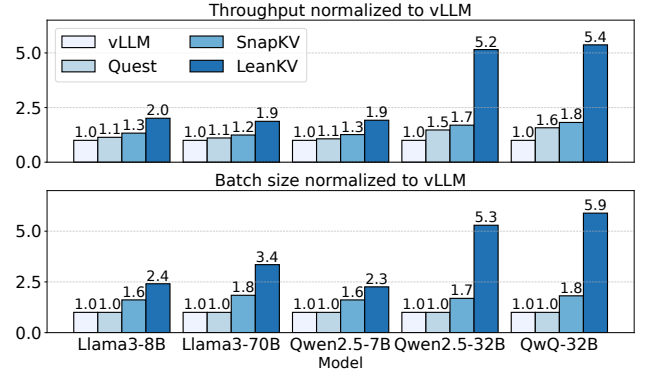


Figure 14: Throughput and achieved batch size.

the entire KV cache without reducing memory usage. Its speedup comes primarily from faster attention computation, as it processes only a subset of tokens deemed important. However, the process of estimating token importance incurs additional overhead, limiting the overall efficiency of Quest.

## 8 Conclusion

We propose LeanKV, a framework to enhance LLM serving efficiency by exploiting three levels of differentiation in KV cache: differentiated precision for keys and values, hierarchical compression based on varying token importance, and per-head dynamic sparsity. At the core of LeanKV is the parallel KV compaction technique that efficiently handles irregular memory requirements across requests and attention heads, effectively translating memory savings into performance gains. Our evaluation shows that LeanKV is able to compress the KV cache by 2.7× to 5.7× without compromising accuracy on complex workloads that require sophisticated reasoning and long-generation capabilities, and enhances throughput by 1.9× to 5.4×.

## References

- [1] FasterTransformer. <https://github.com/NVIDIA/FasterTransformer>.
- [2] FlashInfer: Kernel Library for LLM Serving. <https://github.com/flashinfer-ai/flashinfer>.
- [3] Aime 2024. <https://huggingface.co/datasets/AI-MO/aimo-validation-aime>, 2024.
- [4] ACHIAM, J., ADLER, S., AGARWAL, S., AHMAD, L., AKKAYA, I., ALEMAN, F. L., ALMEIDA, D., ALTENSCHMIDT, J., ALTMAN, S., ANADKAT, S., ET AL. Gpt-4 technical report. *arXiv preprint arXiv:2303.08774* (2023).
- [5] AINSLIE, J., LEE-THORP, J., DE JONG, M., ZEMLYANSKIY, Y., LEBRÓN, F., AND SANGLAI, S. Gqa: Training generalized multi-query transformer models from multi-head checkpoints. *arXiv preprint arXiv:2305.13245* (2023).
- [6] AMINABADI, R. Y., RAJBHANDARI, S., AWAN, A. A., LI, C., LI, D., ZHENG, E., RUWASE, O., SMITH, S., ZHANG, M., RASLEY, J., ET AL. Deepspeed-inference: enabling efficient inference of transformer models at unprecedented scale. In *SC22: International Conference for High Performance Computing, Networking, Storage and Analysis* (2022), IEEE, pp. 1–15.
- [7] AUSTIN, J., ODENA, A., NYE, M., BOSMA, M., MICHALEWSKI, H., DOHAN, D., JIANG, E., CAI, C., TERRY, M., LE, Q., ET AL. Program synthesis with large language models. *arXiv preprint arXiv:2108.07732* (2021).
- [8] BAI, Y., LV, X., ZHANG, J., LYU, H., TANG, J., HUANG, Z., DU, Z., LIU, X., ZENG, A., HOU, L., ET AL. Longbench: A bilingual, multitask benchmark for long context understanding. *arXiv preprint arXiv:2308.14508* (2023).
- [9] BROWN, T. B. Language models are few-shot learners. *arXiv preprint arXiv:2005.14165* (2020).
- [10] CAI, Z., ZHANG, Y., GAO, B., LIU, T., LU, K., XIONG, W., DONG, Y., CHANG, B., HU, J., AND XIAO, W. Pyramidkv: Dynamic kv cache compression based on pyramidal information funneling. *arXiv preprint arXiv:2406.02069* (2024).
- [11] CHEN, M., TWOREK, J., JUN, H., YUAN, Q., PINTO, H. P. D. O., KAPLAN, J., EDWARDS, H., BURDA, Y., JOSEPH, N., BROCKMAN, G., ET AL. Evaluating large language models trained on code. *arXiv preprint arXiv:2107.03374* (2021).
- [12] CHIANG, W.-L., ZHENG, L., SHENG, Y., ANGELOPOULOS, A. N., LI, T., LI, D., ZHANG, H., ZHU, B., JORDAN, M., GONZALEZ, J. E., ET AL. Chatbot arena: An open platform for evaluating llms by human preference. *arXiv preprint arXiv:2403.04132* (2024).
- [13] COBBE, K., KOSARAJU, V., BAVARIAN, M., CHEN, M., JUN, H., KAISER, L., PLAPPERT, M., TWOREK, J., HILTON, J., NAKANO, R., ET AL. Training verifiers to solve math word problems. *arXiv preprint arXiv:2110.14168* (2021).
- [14] DAO, T. Flashattention-2: Faster attention with better parallelism and work partitioning. *arXiv preprint arXiv:2307.08691* (2023).
- [15] DAO, T., FU, D., ERMON, S., RUDRA, A., AND RÉ, C. Flashattention: Fast and memory-efficient exact attention with io-awareness. *Advances in Neural Information Processing Systems 35* (2022), 16344–16359.
- [16] DETTMERS, T., LEWIS, M., BELKADA, Y., AND ZETTLEMOYER, L. Gpt3. int8 (): 8-bit matrix multiplication for transformers at scale. *Advances in Neural Information Processing Systems 35* (2022), 30318–30332.
- [17] DUBEY, A., JAUHRI, A., PANDEY, A., KADIAN, A., AL-DAHLE, A., LETMAN, A., MATHUR, A., SCHELTEN, A., YANG, A., FAN, A., ET AL. The llama 3 herd of models. *arXiv preprint arXiv:2407.21783* (2024).
- [18] FANG, J., YU, Y., ZHAO, C., AND ZHOU, J. Turbotransformers: an efficient gpu serving system for transformer models. In *Proceedings of the 26th ACM SIGPLAN Symposium on Principles and Practice of Parallel Programming* (2021), pp. 389–402.
- [19] GAO, P., YU, L., WU, Y., AND LI, J. Low latency rnn inference with cellular batching. In *Proceedings of the Thirteenth EuroSys Conference* (2018), pp. 1–15.
- [20] GE, S., ZHANG, Y., LIU, L., ZHANG, M., HAN, J., AND GAO, J. Model tells you what to discard: Adaptive kv cache compression for llms. *arXiv preprint arXiv:2310.01801* (2023).
- [21] GITHUB. Github copilot. <https://github.com/features/copilot>, 2023.
- [22] GUO, C., TANG, J., HU, W., LENG, J., ZHANG, C., YANG, F., LIU, Y., GUO, M., AND ZHU, Y. Olive: Accelerating large language models via hardware-friendly outlier-victim pair quantization. In *Proceedings of the 50th Annual International Symposium on Computer Architecture* (2023), pp. 1–15.

[23] GUO, D., YANG, D., ZHANG, H., SONG, J., ZHANG, R., XU, R., ZHU, Q., MA, S., WANG, P., BI, X., ET AL. Deepseek-r1: Incentivizing reasoning capability in llms via reinforcement learning. *arXiv preprint arXiv:2501.12948* (2025).

[24] GUO, D., ZHU, Q., YANG, D., XIE, Z., DONG, K., ZHANG, W., CHEN, G., BI, X., WU, Y., LI, Y., ET AL. Deepseek-coder: When the large language model meets programming—the rise of code intelligence. *arXiv preprint arXiv:2401.14196* (2024).

[25] HAN, M., ZHANG, H., CHEN, R., AND CHEN, H. Microsecond-scale preemption for concurrent {GPU-accelerated} {DNN} inferences. In *16th USENIX Symposium on Operating Systems Design and Implementation (OSDI 22)* (2022), pp. 539–558.

[26] HENDRYCKS, D., BURNS, C., BASART, S., ZOU, A., MAZEIKA, M., SONG, D., AND STEINHARDT, J. Measuring massive multitask language understanding. *arXiv preprint arXiv:2009.03300* (2020).

[27] HOOPER, C., KIM, S., MOHAMMADZADEH, H., MAHONEY, M. W., SHAO, Y. S., KEUTZER, K., AND GHOLAMI, A. Kvquant: Towards 10 million context length llm inference with kv cache quantization. *arXiv preprint arXiv:2401.18079* (2024).

[28] HUI, B., YANG, J., CUI, Z., YANG, J., LIU, D., ZHANG, L., LIU, T., ZHANG, J., YU, B., LU, K., ET AL. Qwen2. 5-coder technical report. *arXiv preprint arXiv:2409.12186* (2024).

[29] JAECH, A., KALAI, A., LERER, A., RICHARDSON, A., EL-KISHKY, A., LOW, A., HELYAR, A., MADRY, A., BEUTEL, A., CARNEY, A., ET AL. Openai o1 system card. *arXiv preprint arXiv:2412.16720* (2024).

[30] JIANG, A. Q., SABLAYROLLES, A., ROUX, A., MENSCH, A., SAVARY, B., BAMFORD, C., CHAPLOT, D. S., CASAS, D. D. L., HANNA, E. B., BRESSAND, F., ET AL. Mixtral of experts. *arXiv preprint arXiv:2401.04088* (2024).

[31] KAO, S.-C., SUBRAMANIAN, S., AGRAWAL, G., YAZDANBAKHS, A., AND KRISHNA, T. Flat: An optimized dataflow for mitigating attention bottlenecks. In *Proceedings of the 28th ACM International Conference on Architectural Support for Programming Languages and Operating Systems, Volume 2* (2023), pp. 295–310.

[32] KWON, W., LI, Z., ZHUANG, S., SHENG, Y., ZHENG, L., YU, C. H., GONZALEZ, J., ZHANG, H., AND STOICA, I. Efficient memory management for large language model serving with pagedattention. In *Proceedings of the 29th Symposium on Operating Systems Principles* (2023), pp. 611–626.

[33] LEE, W., LEE, J., SEO, J., AND SIM, J. {InfiniGen}: Efficient generative inference of large language models with dynamic {KV} cache management. In *18th USENIX Symposium on Operating Systems Design and Implementation (OSDI 24)* (2024), pp. 155–172.

[34] LEWKOWYCZ, A., ANDREASSEN, A., DOHAN, D., DYER, E., MICHALEWSKI, H., RAMASESH, V., SLOANE, A., ANIL, C., SCHLAG, I., GUTMAN-SOLO, T., ET AL. Solving quantitative reasoning problems with language models. *Advances in Neural Information Processing Systems 35* (2022), 3843–3857.

[35] LI, Y., HUANG, Y., YANG, B., VENKITESH, B., LOCATELLI, A., YE, H., CAI, T., LEWIS, P., AND CHEN, D. Snapkv: Llm knows what you are looking for before generation. *arXiv preprint arXiv:2404.14469* (2024).

[36] LI, Z., ZHENG, L., ZHONG, Y., LIU, V., SHENG, Y., JIN, X., HUANG, Y., CHEN, Z., ZHANG, H., GONZALEZ, J. E., ET AL. {AlpaServe}: Statistical multiplexing with model parallelism for deep learning serving. In *17th USENIX Symposium on Operating Systems Design and Implementation (OSDI 23)* (2023), pp. 663–679.

[37] LIN, Y., TANG, H., YANG, S., ZHANG, Z., XIAO, G., GAN, C., AND HAN, S. Qserve: W4a8kv4 quantization and system co-design for efficient llm serving. *arXiv preprint arXiv:2405.04532* (2024).

[38] LIU, A., FENG, B., WANG, B., WANG, B., LIU, B., ZHAO, C., DENGR, C., RUAN, C., DAI, D., GUO, D., ET AL. Deepseek-v2: A strong, economical, and efficient mixture-of-experts language model. *arXiv preprint arXiv:2405.04434* (2024).

[39] LIU, J., XIA, C. S., WANG, Y., AND ZHANG, L. Is your code generated by chatGPT really correct? rigorous evaluation of large language models for code generation. In *Thirty-seventh Conference on Neural Information Processing Systems* (2023).

[40] LIU, Z., DESAI, A., LIAO, F., WANG, W., XIE, V., XU, Z., KYRILLIDIS, A., AND SHRIVASTAVA, A. Scissorhands: Exploiting the persistence of importance hypothesis for llm kv cache compression at test time. *Advances in Neural Information Processing Systems 36* (2024).

[41] LIU, Z., YUAN, J., JIN, H., ZHONG, S., XU, Z., BRAVERMAN, V., CHEN, B., AND HU, X. Kivi: A tuning-free asymmetric 2bit quantization for kv cache. *arXiv preprint arXiv:2402.02750* (2024).

[42] MERITY, S., XIONG, C., BRADBURY, J., AND SOCHER, R. Pointer sentinel mixture models. *arXiv preprint arXiv:1609.07843* (2016).

[43] NAGEL, M., FOURNARAKIS, M., AMJAD, R. A., BONDARENKO, Y., VAN BAALEN, M., AND BLANKEVOORT, T. A white paper on neural network quantization. *arXiv preprint arXiv:2106.08295* (2021).

[44] NAKANO, K. An optimal parallel prefix-sums algorithm on the memory machine models for gpus. In *International Conference on Algorithms and Architectures for Parallel Processing* (2012), Springer, pp. 99–113.

[45] NVIDIA. Nvidia l40 datasheet. <https://www.nvidia.com/content/dam/en-zz/Solutions/design-visualization/support-guide/NVIDIA-L40-Datasheet-January-2023.pdf>, 2023.

[46] OUYANG, L., WU, J., JIANG, X., ALMEIDA, D., WAINWRIGHT, C., MISHKIN, P., ZHANG, C., AGARWAL, S., SLAMA, K., RAY, A., ET AL. Training language models to follow instructions with human feedback. *Advances in neural information processing systems* 35 (2022), 27730–27744.

[47] POPE, R., DOUGLAS, S., CHOWDHERY, A., DEVLIN, J., BRADBURY, J., HEEK, J., XIAO, K., AGRAWAL, S., AND DEAN, J. Efficiently scaling transformer inference. *Proceedings of Machine Learning and Systems* 5 (2023), 606–624.

[48] REIN, D., HOU, B. L., STICKLAND, A. C., PETTY, J., PANG, R. Y., DIRANI, J., MICHAEL, J., AND BOWMAN, S. R. Gpqa: A graduate-level google-proof q&a benchmark. In *First Conference on Language Modeling* (2024).

[49] SAAB, K., TU, T., WENG, W.-H., TANNO, R., STUTZ, D., WULCZYN, E., ZHANG, F., STROTHER, T., PARK, C., VEDADI, E., ET AL. Capabilities of gemini models in medicine. *arXiv preprint arXiv:2404.18416* (2024).

[50] SHAO, Z., WANG, P., ZHU, Q., XU, R., SONG, J., ZHANG, M., LI, Y., WU, Y., AND GUO, D. Deepseekmath: Pushing the limits of mathematical reasoning in open language models. *arXiv preprint arXiv:2402.03300* (2024).

[51] SHAZER, N. Fast transformer decoding: One write-head is all you need. *arXiv preprint arXiv:1911.02150* (2019).

[52] SHENG, Y., ZHENG, L., YUAN, B., LI, Z., RYABININ, M., CHEN, B., LIANG, P., RÉ, C., STOICA, I., AND ZHANG, C. Flexgen: High-throughput generative inference of large language models with a single gpu. In *International Conference on Machine Learning* (2023), PMLR, pp. 31094–31116.

[53] SHI, Y., YANG, Z., XUE, J., MA, L., XIA, Y., MIAO, Z., GUO, Y., YANG, F., AND ZHOU, L. Welder: Scheduling deep learning memory access via tile-graph. In *17th USENIX Symposium on Operating Systems Design and Implementation (OSDI 23)* (2023), pp. 701–718.

[54] SHOEYBI, M., PATWARY, M., PURI, R., LEGRESLEY, P., CASPER, J., AND CATANZARO, B. Megatron-lm: Training multi-billion parameter language models using model parallelism. *arXiv preprint arXiv:1909.08053* (2019).

[55] TAGHANAKI, S. A., KHANI, A., AND KHASAHMADI, A. Mmlu-pro+: Evaluating higher-order reasoning and shortcut learning in llms. *arXiv preprint arXiv:2409.02257* (2024).

[56] TANG, J., ZHAO, Y., ZHU, K., XIAO, G., KASIKCI, B., AND HAN, S. Quest: Query-aware sparsity for efficient long-context llm inference. *arXiv preprint arXiv:2406.10774* (2024).

[57] TEAM, G., ANIL, R., BORGEAUD, S., WU, Y., ALAYRAC, J.-B., YU, J., SORICUT, R., SCHALKWYK, J., DAI, A. M., HAUTH, A., ET AL. Gemini: a family of highly capable multimodal models. *arXiv preprint arXiv:2312.11805* (2023).

[58] TEAM, Q. Qwq-32b: Embracing the power of reinforcement learning, March 2025.

[59] TEAM, T. V. Vicuna: An open-source chatbot impressing gpt-4 with 90

[60] TOUVRON, H., MARTIN, L., STONE, K., ALBERT, P., ALMAHAIRI, A., BABAEI, Y., BASHLYKOV, N., BATRA, S., BHARGAVA, P., BHOSALE, S., ET AL. Llama 2: Open foundation and fine-tuned chat models. *arXiv preprint arXiv:2307.09288* (2023).

[61] VASWANI, A. Attention is all you need. *Advances in Neural Information Processing Systems* (2017).

[62] WOLF, T., DEBUT, L., SANH, V., CHAUMOND, J., DELANGUE, C., MOI, A., CISTAC, P., RAULT, T., LOUF, R., FUNTOWICZ, M., ET AL. Transformers: State-of-the-art natural language processing. In *Proceedings of the 2020 conference on empirical methods in natural language processing: system demonstrations* (2020), pp. 38–45.

[63] XIAO, G., TANG, J., ZUO, J., GUO, J., YANG, S., TANG, H., FU, Y., AND HAN, S. Duoattention: Efficient long-context llm inference with retrieval and streaming heads. *arXiv preprint arXiv:2410.10819* (2024).

[64] XIAO, G., TIAN, Y., CHEN, B., HAN, S., AND LEWIS, M. Efficient streaming language models with attention sinks. *arXiv preprint arXiv:2309.17453* (2023).

[65] XIE, Y., WU, J., TU, H., YANG, S., ZHAO, B., ZONG, Y., JIN, Q., XIE, C., AND ZHOU, Y. A preliminary study of o1 in medicine: Are we closer to an ai doctor? *arXiv preprint arXiv:2409.15277* (2024).

[66] YANG, Y., ZHAO, L., LI, Y., ZHANG, H., LI, J., ZHAO, M., CHEN, X., AND LI, K. Infless: a native serverless system for low-latency, high-throughput inference. In *Proceedings of the 27th ACM International Conference on Architectural Support for Programming Languages and Operating Systems* (2022), pp. 768–781.

[67] YU, G.-I., JEONG, J. S., KIM, G.-W., KIM, S., AND CHUN, B.-G. Orca: A distributed serving system for {Transformer-Based} generative models. In *16th USENIX Symposium on Operating Systems Design and Implementation (OSDI 22)* (2022), pp. 521–538.

[68] ZHANG, H., TANG, Y., KHANDELWAL, A., AND STOICA, I. {SHEPHERD}: Serving {DNNs} in the wild. In *20th USENIX Symposium on Networked Systems Design and Implementation (NSDI 23)* (2023), pp. 787–808.

[69] ZHANG, Z., SHENG, Y., ZHOU, T., CHEN, T., ZHENG, L., CAI, R., SONG, Z., TIAN, Y., RÉ, C., BARRETT, C., ET AL. H2o: Heavy-hitter oracle for efficient generative inference of large language models. *Advances in Neural Information Processing Systems 36* (2024).

[70] ZHAO, Y., LIN, C.-Y., ZHU, K., YE, Z., CHEN, L., ZHENG, S., CEZE, L., KRISHNAMURTHY, A., CHEN, T., AND KASIKCI, B. Atom: Low-bit quantization for efficient and accurate llm serving. *Proceedings of Machine Learning and Systems 6* (2024), 196–209.

[71] ZHONG, T., LIU, Z., PAN, Y., ZHANG, Y., ZHOU, Y., LIANG, S., WU, Z., LYU, Y., SHU, P., YU, X., ET AL. Evaluation of openai o1: Opportunities and challenges of agi. *arXiv preprint arXiv:2409.18486* (2024).